PAPER

Check for updates

Study on the formation and properties of red blood cell-like Fe₃O₄/TbLa₃(Bim)₁₂/PLGA composite particles

Ping Li, [iD] †[ab] Bing Qi,†[ab] Kun Li,[ab] Junwei Xu, [iD] [ab] Meili Liu,[ab] Xuenan Gu,[ab] Xufeng Niu [iD] [ab] and Yubo Fan*[abc]

Besides the particle size and surface performance, the shape also plays a key role in drug delivery systems. Red blood cells are the most abundant blood cells in the human body, and are excellent oxygen carriers, due to their unique biconcave discoid shape. In this study, red blood cell (RBC)-like Fe_3O_4/TbLa$_3$(Bim)$_{12}$/ poly(lactic-co-glycolic acid) (PLGA) composite particles, with magnetic response and bioimaging functions, were prepared by electrospraying. Various electrospraying parameters, such as solvent, PLGA concentration, collecting distance and solution flow rate were investigated in detail to attempt to obtain RBC-like composite particles. The size distribution, morphology, structure, and hydrophobicity–hydrophilicity of particles were characterized. The results revealed the RBC-like Fe_3O_4/TbLa$_3$(Bim)$_{12}$/ PLGA composite particles exhibited a strong green fluorescence and good magnetic behavior even when incubated with cells. Furthermore, the intensity of the magnetization and fluorescence can be adjusted by changing the contents of Fe_3O_4 and TbLa$_3$(Bim)$_{12}$. The effect on cell viability of the RBC-like Fe_3O_4/TbLa$_3$(Bim)$_{12}$/PLGA composite particles was evaluated in A549 cells and RBCs, and it was determined to have low cytotoxicity and excellent blood biocompatibility, suggesting that it is a promising candidate for application in drug delivery, targeting and tracking.

1. Introduction

In the biomaterials field, polymeric particles offer the potential to improve biomedical applications, such as targeted drug delivery, vaccination and bioimaging,[1–3] and have already produced a series of significant results.[4–7] Most polymeric particles are spherical carriers because of simplicity and versatility of the fabrication process. However, some studies have found that the shape of particles played important roles in evading phagocytosis, margination and targeting.[8–10] Geng et al.[11] reported a kind of copolymer micelle assembly, consisting of polyethyleneglycol, polyethylethylene and poly-caprolactone, which exhibited about ten times longer circulation time in rodents than the spherical counterpart with similar chemistry. Additionally, they proved that the assembly with paclitaxel could be effectively used to treat the tumor in mice. Godin et al.[12] found that in breast tumor, discoidal

particles would more likely stick to the vessel walls, and the accumulation of discoidal porous silicons was five times higher compared to the spherical ones with the same diameter. In addition, some theoretical model studies also showed that non-spherical carriers were useful in cellular internalization and vascular dynamics. Decuzzi[13] calculated the interaction between cylindrical particles and the cell membrane and found that only particles with intermediate aspect ratio could be fully wrapped and eventually internalized. In another study, Decuzzi[14] analyzed the specific adhesive interaction between a non-spherical particle and a cell layer under a linear shear flow and the result showed that oblate particles adhered more effectively to biological substrate than spherical ones.

Red blood cells (RBCs) with unique biconcave discoid morphology represent a remarkable example of shape enabling the implementation of sophisticated biological functionalities.[15] For example, RBCs can flow through small bore capillary.[16] Moreover, the distinctive biconcave discoid shape gives RBCs the ability to protect themselves from being filtered by the spleen.[17] Accordingly, developing a kind of RBC mimicking carrier with biconcave discoid can be expected to greatly enhance the flow and accumulation of drug in body.

In current studies, the main methods to prepare RBC-like particles are the layer by layer (LBL) method, particle replication in non-wetting templates (PRINT) method, stretching/compressing method, and electrospraying. Kozlovskaya V.

[a]School of Biological Science and Medical Engineering, Key Laboratory for Biomechanics and Mechanobiology, Ministry of Education, Beihang University, Beijing, 100083, China. E-mail: yubofan@buaa.edu.cn

[b]Beijing Advanced Innovation Centre for Biomedical Engineering, Beihang University, Beijing, 100083, China

[c]Beijing Key Laboratory of Rehabilitation Technical Aids for Old-Age Disability, National Research Center for Rehabilitation Technical Aids, Beijing, 100176, China

† P. Li and B. Qi contributed equally to this work.

et al.[18] fabricated polymethyl methacrylate (PMMA) discoidal hydrogel capsules to study the internalization of RBCs using the LBL approach, and Merkel T. J. *et al.*[19] prepared RBC hydrogel micro-particles by the PRINT method to mimic the mechano-biological properties. However, a template prepared *via* traditional photolithography was necessary for the two methods mentioned above. Also, Fan J. B. *et al.*[20] synthesized anisotropic biodegradable poly(lactic-*co*-glycolic acid) (PLGA) nanoparticles using the stretching/compressing technique to study the controllable drug release. However, this method required the fabrication of spherical particles at first, then the compressing force was applied to obtain the desire shape like RBC particles.

Electrospraying is a well-established technique for generating mono-dispersed size droplets under an electrical force. It is a one-step, inexpensive and versatile method for preparing particles, which allows to obtain particles with various shapes by adjusting a series of experimental parameters.[21–24] Hayashi, K. *et al.*[25] successfully prepared RBC particles, with magnetic resonance and fluorescence imaging functions, using cellulose derivatives by electrospraying. They pointed out that the sheet structure of the cellulose derivatives contributed to the formation of the RBC morphology, while the polymers without a sheet structure like dextran, polyethylene glycol, and PMMA could not produce a RBC shape. Park, C. H. *et al.*[26] synthesized mono-disperse RBC-like polyurethane (PAN) particles by electrospraying and he attributed the morphology to the asymmetry diffusivities. When the diffusivity of PAN solutions diffusing into the air/droplet interface was lower than that of solvents diffusing into the surrounding air, the RBC-like particles could be produced. Ju, X. *et al.*[27] prepared RBC-shaped chitosan micro-particles using wet-electrospray. In their study, a glass chamber filled with oil and a magnetic stirrer were required as a coagulating bath. They suggested that the key to produce RBC structure was the interaction between the evaporable solvent of the precursor solution and the diffusible solvent in the coagulating bath.

There is an increasing number of multifunctional materials that have been explored, such as magnetic-fluorescent bifunctional materials,[28] electrical-magnetic bifunctional materials,[29] fluorescent-electrical bifunctional materials[30] and electrical-magnetic-fluorescent trifunctional materials.[31] However, the RBC-like multifunctional PLGA composite particles have not been thoroughly studied, especially *via* the electrospraying technique. Rare earth (RE) elements exhibit low toxicity, high luminescence quantum yield, narrow bandwidth, large Stokes shifts and ligand-dependent luminescence sensitization. These properties allow RE elements to avoid the intrinsic limitations of traditional dyes, such as short fluorescent lifetime, relatively high bio-toxicity and low chemical stability.[32] Accordingly, they have been used as fluorescent labeling materials of drug delivery system (DDS). In our previous study, drug complexes with dual RE ions were successfully prepared. The synthesized complexes did not only increase the fluorescent intensity of the materials, but also greatly enhanced the accuracy of the drug tracing due to the existence of coordinate bond.

In this study, we aimed to generate RBC-like bifunctional particles as DDS carriers. To this end, the dual RE complex TbLa$_3$(Bim)$_{12}$ was synthesized as fluorescent material and Fe$_3$O$_4$ magnetic nanoparticles (MNPs) were used as the magnetic materials. We investigated the factors influencing the formation of RBC-like bifunctional particles in detail, including solvents, PLGA concentrations, collecting distances and flow rates of the solutions. The morphology, size distribution, structure, magnetic behaviour, fluorescent performance and hydrophobicity–hydrophilicity of the composite particles were studied. The effect of RBC-like Fe$_3$O$_4$/TbLa$_3$(Bim)$_{12}$/PLGA composite particles at different concentrations on the viability of the adenocarcinoma human alveolar basal epithelial A549 cells was evaluated. The hemolytic activity and protein binding were also evaluated. The results suggested that the RBC-like bifunctional Fe$_3$O$_4$/TbLa$_3$(Bim)$_{12}$/PLGA composite particles could have potential application in drug delivery, targeting and tracking.

2. Experimental

2.1 Materials

PLGA ($M_w = 1 \times 10^5$, LA : GA = 85 : 15) was purchased from Jinan Daigang Biotechnology Co., LTD (China). La$_2$O$_3$ (99%), Tb$_4$O$_7$ (99%) and benzimidazole (Bim) were purchased from Sinopharm Chemical Reagent Co., LTD (China). NaOH, FeCl$_3$·6H$_2$O and FeCl$_2$·4H$_2$O were provided by Xilong Chemical Co., LTD (China). Hydrogen peroxide (H$_2$O$_2$, 30%), hydrochloric acid (HCl), trichloromethane (CHCl$_3$), tetrahydrofuran (THF), dichloromethane (CH$_2$Cl$_2$) and absolute ethylalcohol were provided by Beijing Chemical Works (China). Hexafluoroisopropanol (HFIP) was purchased from Aladdin Industrial Corporation. All reagents involved in this work were of analytical grade and directly used as-received without any further purification.

2.2 Preparation of Fe$_3$O$_4$ MNPs

Fe$_3$O$_4$ MNPs were obtained *via* a facile co-precipitation synthetic method. Briefly, 9.73 g FeCl$_3$·6 H$_2$O, 3.98 g FeCl$_2$·4H$_2$O and 6.67 g NaOH were added in 300 mL of deionized water, then stirred vigorously at 60 °C for 4 h and black precipitate was got. 0.03 M HCl was added in the black precipitate and the mixture was dispersed by ultrasound. Finally, the precipitate was washed several times with deionized water and dried under vacuum at 60 °C for 12 h.

2.3 Synthesis of RE complex of TbLa$_3$(Bim)$_{12}$

The synthesis of RE complex was carry out according to the method of Li, P. *et al.*[33] To be specific, 1 g La$_2$O$_3$ was dissolved in 10 mL concentrated HCl, 1 g Tb$_4$O$_7$ was dissolved in 10 mL concentrated HCl with appropriate amount of 30% H$_2$O$_2$. After evaporating of excess HCl, the white powders LaCl$_3$ and TbCl$_3$ were obtained. Then LaCl$_3$, TbCl$_3$ and Bim with molar ratio of 1 : 3 : 12 were dissolved in 80 mL ethanol. The mixture solutions were heated with thorough agitation at 60 °C for 6 h and separated by centrifugation. At last, the deposit was dried in the oven at 65 °C for 12 h.
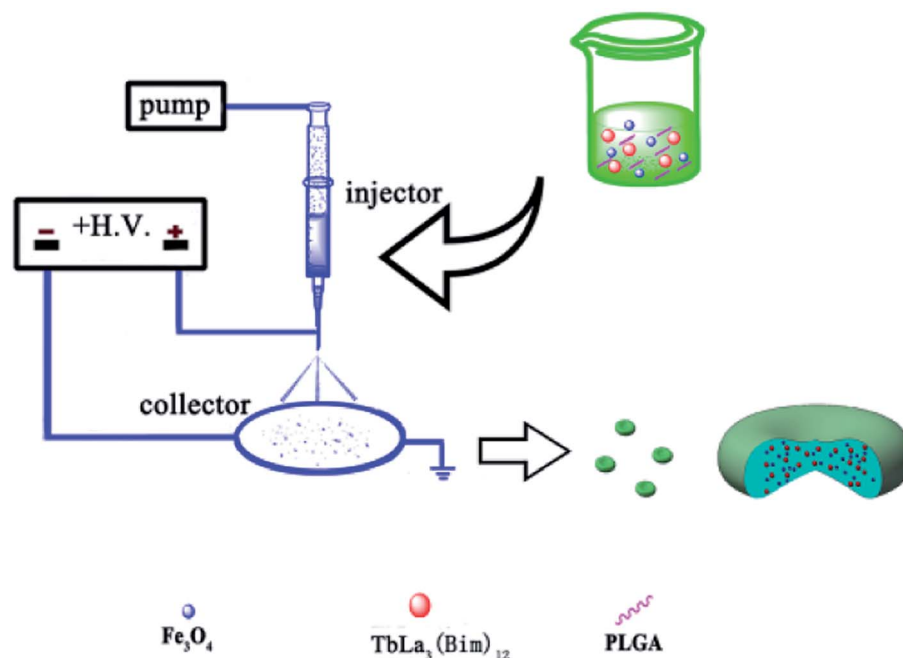
Fig. 1 Schematic illustration of the preparation of the RBC-like magnetic-fluorescent bifunctional Fe_3O_4/$TbLa_3(Bim)_{12}$/PLGA composite particles.

2.4 Fabrication of RBC-like magnetic-fluorescent Fe_3O_4/$TbLa_3(Bim)_{12}$/PLGA composite particles *via* electrospraying

To prepare the RBC-like Fe_3O_4/$TbLa_3(Bim)_{12}$/PLGA composite particles, an electrospraying setup was employed. The experimental process was schematically illustrated in Fig. 1. The precursor components of PLGA, $TbLa_3(Bim)_{12}$ and Fe_3O_4 MNPs were loaded into a 1 mL syringe with a stainless needle and the high voltage was set at 6–9 kV. An aluminum foil was used as the collector, which was placed at a certain distance away from the spinneret. The whole process was performed at room temperature. The influence of the experimental parameters, including the different solvents, PLGA concentration, collecting distance and flow rate of the solutions, were investigated during the formation of the RBC-like Fe_3O_4/$TbLa_3(Bim)_{12}$/PLGA composite particles.

2.4.1 The influence of solvent on RBC-like Fe_3O_4/$TbLa_3(Bim)_{12}$/PLGA composite particles. The different components, specifically 50 mg of Fe_3O_4 MNPs, 125 mg of PLGA and 100 mg of $TbLa_3(Bim)_{12}$ were dissolved in 5 mL of different solvents, including $CHCl_3$, THF, CH_2Cl_2 and HFIP. After stirring for 4 h, the precursor solutions were prepared. During electrospraying, the flow rate was 0.8 mL h^{-1} and the collecting distance was 15 cm.

2.4.2 The influence of the PLGA concentration (%, w/v) on the RBC-like Fe_3O_4/$TbLa_3(Bim)_{12}$/PLGA composite particles. The precursor solutions were prepared by dissolving 50 mg of Fe_3O_4 MNPs, 100 mg of $TbLa_3(Bim)_{12}$ and different amounts of PLGA in 5 mL THF. After stirring for 4 h, the parameters used for electrospraying were: flow rate at 0.8 mL h^{-1} and collecting distance of 15 cm. The different PLGA concentrations were 0.625, 1.25, 2.5, 3.75, 5, 7.5, 10 and 15%, respectively.

2.4.3 The influence of the collecting distance on the RBC-like Fe_3O_4/$TbLa_3(Bim)_{12}$/PLGA composite particles. The precursor solution with 2.5% PLGA was chosen to conduct the study in impact of the collecting distance. The evaluated collecting distances of electrospraying were 5, 15, 25, 35 and 45 cm. The flow rate was 0.8 mL h^{-1}.

2.4.4 The influence of flow rate of solutions on RBC-like Fe_3O_4/$TbLa_3(Bim)_{12}$/PLGA composite particles. The precursor solution with 2.5% PLGA was also used to conduct the study on the influence of flow rates. The evaluated flow rates of electrospraying were 0.10, 0.40, 1.60, 2.40, 3.20, 4.80, 6.00 and 7.20 mL h^{-1}. The collecting distance was 15 cm.

2.4.5 The preparation of RBC-like Fe_3O_4/$TbLa_3(Bim)_{12}$/PLGA composite particles containing different amounts of Fe_3O_4 and $TbLa_3(Bim)_{12}$. The optimal electrospraying conditions for generating RBC-like particles were first determined. Then, we prepared several kinds of RBC-like particles with different contents of Fe_3O_4 MNPs and $TbLa_3(Bim)_{12}$. The detailed dosages of materials are shown in Table 1.

Table 1 Compositions of the precursor solutions

Sample	Fe_3O_4 (mg)	$TbLa_3(Bim)_{12}$ (mg)	PLGA (mg)	Solvent (5 mL)
S1	50	100	125	THF
S2	100	100	125	THF
S3	150	100	125	THF
S4	100	50	125	THF
S5	100	100	125	THF
S6	100	150	125	THF

2.5 Cell experiments

2.5.1 Cell culture. A549 cells were obtained from Institute of Basic Medical Sciences (IBMS) of Chinese Academy of Medical Sciences (CAMS). Fetal bovine serum (FBS) was got from Zhejiang Tianhang Biotechnology Co., LTD. All other cell culture related reagents were purchased from Beijing Solarbio Science & Technology Co., LTD. Cells were grown in normal RPMI-1640 culture medium with 10% FBS and 1% penicillin/streptomycin.

2.5.2 Cell viability. The *in vitro* cell viability was measured using a standard CCK-8 assay. A549 cells were seeded in a 96-well plate at a density of 8000 cells per well and cultured in 1640 RPMI medium in 5% CO_2 at 37 °C for 24 h. Then different concentrations (7.81, 31.25, 62.5, 125, 250, 500, 1000 μg mL^{-1}) of the RBC-like Fe_3O_4/TbLa$_3$(Bim)$_{12}$/PLGA particles (S6 in Table 1) were added to the cell culture medium, and incubated with the cells for 24 h. After incubation, the medium containing the particles was removed from each well and 100 μL of a solution, consisting of 10 μL of the CCK-8 reagent solution and 90 μL of cell culture medium, were added into each well and incubated for another 4 h. The absorbance of each well in the plate was measured using a micro-plate reader at the wavelength of 450 nm and the data was used to calculate the cell viability.

2.5.3 Cell imaging. The cell imaging capability of RBC-like Fe_3O_4/TbLa$_3$(Bim)$_{12}$/PLGA particles was testified using A549 cells. Briefly, A549 cells were seeded in 60 mm Petri dishes with 4 mL RPMI-1640 culture medium and grew for 24 h as a monolayer. Then the cells were washed with PBS solution, and a certain amount of Fe_3O_4/TbLa$_3$(Bim)$_{12}$/PLGA composite particles (S6 in Table 1) diluted in medium were added,

incubating for 24 h. The images were performed with a fluorescent microscope.

2.5.4 Magnetic responsiveness. In the magnetic responsive assay, a certain amount of the RBC-like Fe_3O_4/TbLa$_3$(Bim)$_{12}$/PLGA particles (S6 in Table 1) was incubated with A549 cells at 37 °C for 24 h with a ferrite magnet (15 × 88 × 40 mm, 0.72 T) placed near one edge of the Petri dish, and then imaged by fluorescent microscope.

2.6 Hemolysis assay

Hemolytic activity assay was performed according to previous reports.[34] EDTA stabilized rabbit blood samples were freshly obtained from Peking University Health Science Centre (Beijing, China). First, blood was centrifuged at 2000 rpm for 5 min and blood plasma and the surface layer were removed. The remaining RBC pellet was washed with PBS until the supernatant became transparent. 2% RBC suspension was prepared by diluting 1 mL of RBC pellet in 49 mL PBS. Then, 0.8 mL of composite particles solutions in PBS at different concentrations (7.81–250 μg mL^{-1}) was added to 0.2 mL of RBC suspension. Also, 0.8 mL of water and PBS were added in 0.2 mL of RBC suspension as positive and negative control samples, respectively. All the samples were incubated at room temperature for 2 h. The samples were slightly shaken once for every 30 min. After 2 h, the samples were centrifuged at 2000 rpm and 100 mL of supernatants was transferred into a 96-well plate. Absorbance was measured with a micro-plate reader at 570 nm. Hemolysis percentages of the RBCs were calculated using the following formula:

$$\% \text{ Hemolysis} = (\text{abs of sample} - \text{abs of negative control})/(\text{abs of positive control} - \text{abs of negative control})$$

2.7 Non-specific protein binding

Non-specific protein binding of RBC-like Fe_3O_4/TbLa$_3$(Bim)$_{12}$/PLGA particles was performed by BCA Protein Assay Kit. RBC-like particles were incubated with RPMI-1640 culture medium with 10% FBS for 2 h. Then, the particles were diluted by PBS at different concentrations (7.81–500 μg mL^{-1}). All the samples were washed in PBS 2 times to remove the soft corona. Then, samples were dispersed in BCA assay reagents and incubated for 30 min at 37 °C. The resulting solutions were then transferred into a 96-well plate, absorbance was measured at 562 nm using a micro-plate reader.

2.8 Characterization

The morphology of Fe_3O_4, TbLa$_3$(Bim)$_{12}$ and Fe_3O_4/TbLa$_3$(Bim)$_{12}$/PLGA composite particles were observed by transmission electron microscope (TEM, JEM-1200EX, JEOL, Japan) and scanning electron microscope (SEM, Quanta™ 250 FEG SEM, FEI, USA). The size distribution was measured by particle size analyzer (PSA, Zetasizer Nano S and Mastersizer 2000, Malvern, UK). The contact angle and surface tension of particles samples and precursor solutions were recorded using a contact angle measurement
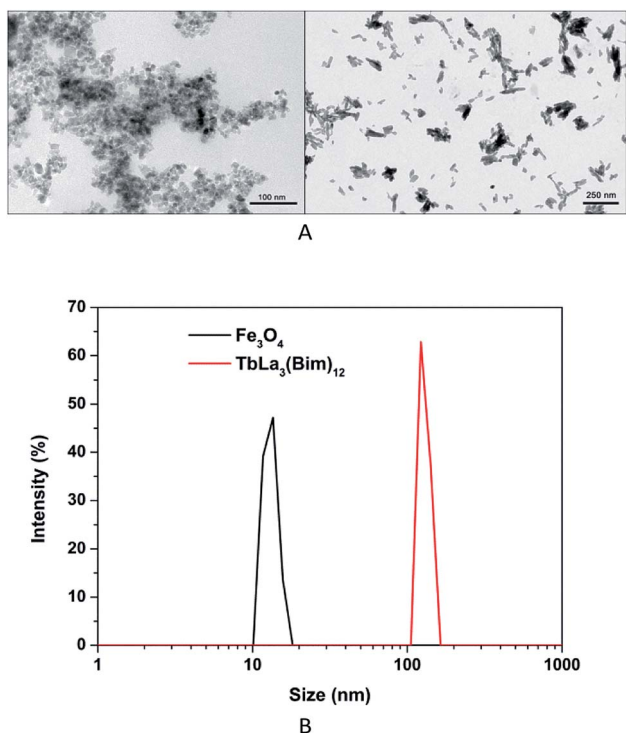

Fig. 2 (A) TEM images of Fe_3O_4 nanoparticles (left) and TbLa$_3$(Bim)$_{12}$ (right); (B) size distribution of Fe_3O_4 nanoparticles and TbLa$_3$(Bim)$_{12}$.
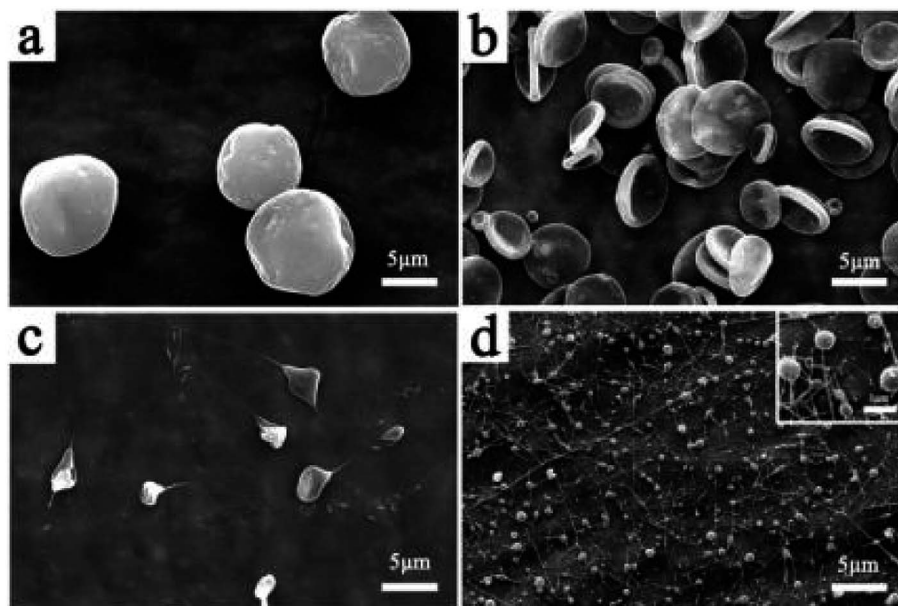
Fig. 3 SEM images of the $Fe_3O_4/TbLa_3(Bim)_{12}$/PLGA composite particles with different solvents. (a) $CHCl_3$, (b) THF, (c) CH_2Cl_2, (d) HFIP.

(JC2000FM, Powereach, China). The viscosity analysis of precursor solution was performed in a cone-plate viscometer (RST-CPS Touch Rheometer, Brookfield, USA). The stability of RBC-like $Fe_3O_4/TbLa_3(Bim)_{12}$/PLGA composite particles was evaluated by UV-VIS-NIR spectrophotometer (UV-VIS-NIR, UV-3600, Shimadzu, Japan). The structure of Bim, $TbLa_3(Bim)_{12}$, PLGA and RBC-like $Fe_3O_4/TbLa_3(Bim)_{12}$/PLGA composite particles were measured by Fourier transform infrared spectroscopy (FTIR-650, Tianjin Gang Dong Technology Development Co., Ltd, China). The phases of Fe_3O_4, Bim, $TbLa_3(Bim)_{12}$ and $Fe_3O_4/TbLa_3(Bim)_{12}$/PLGA composite particles were identified by a X-ray diffraction analysis (XRD, D/MAX-2500, Rigaku, Japan). The magnetic performances of samples were measured by a vibrating sample magnetometer (VSM, Laker Shore 7307, USA) and fluorescent microscope (OLYMBUS, IX73, Japan). The fluorescent properties of samples were investigated by fluorescence spectroscopy (FS5, Edinburgh, UK) and fluorescent microscope. The absorbance was evaluated by a micro-plate reader (Multiskan MK3, Thermo, USA).

2.9 Statistical analysis

Results were expressed as means $\pm$ standard deviation (SD) for repetitive tests. The statistical significance of results between groups was carried out by one-way ANOVA. The statistical analysis was performed with the software SPSS 19.0 at a confidence level of 95%. Differences were considered to be statistically significant for values of $p < 0.05$.

3. Results and discussion

3.1 Fabrication of the RBC-like $Fe_3O_4/TbLa_3(Bim)_{12}$/PLGA composite particles

The size and size distribution of precursors (Fe_3O_4 and $TbLa_3(Bim)_{12}$) were examined by TEM and PSA. The TEM image

(Fig. 2A) and size intensity (Fig. 2B) showed the uniform morphologies of the two precursors. The average hydrodynamic diameter of Fe_3O_4 and $TbLa_3(Bim)_{12}$ was 13.4 and 123.2 nm, respectively.

The morphology and size of PLGA particles can be greatly influenced by various electrospraying parameters, including the solvent, PLGA concentration, collecting distance and flow rate of the solutions.

3.1.1 The influence of solvent on the morphology of the RBC-like $Fe_3O_4/TbLa_3(Bim)_{12}$/PLGA composite particles. The precursor solutions with 125 mg PLGA, 50 mg Fe_3O_4 and 100 mg $TbLa_3(Bim)_{12}$ were electrosprayed with different solvents. The SEM images of the different samples were shown in Fig. 3. Only spherical particles could be prepared when $CHCl_3$ was chosen as solvent (Fig. 3a), while RBC-like particles could be successfully obtained with THF (Fig. 3b). Irregular particles with a short fibres tail were produced using CH_2Cl_2 (Fig. 3c), and small size beads and fibres were prepared with HFIP (Fig. 3d). The difference in the surface tension of the precursor solutions might play an important role in the formation of different shapes. The surface tensions of the four precursor solutions were measured, as shown in Table 2. The jet flow was more likely change to spherical particles, with high surface tension, when the solution was $CHCl_3$. As the surface tension of THF decreased compared with $CHCl_3$, the spheres collapsed, thereby forming RBC particles. When the value of the surface tension
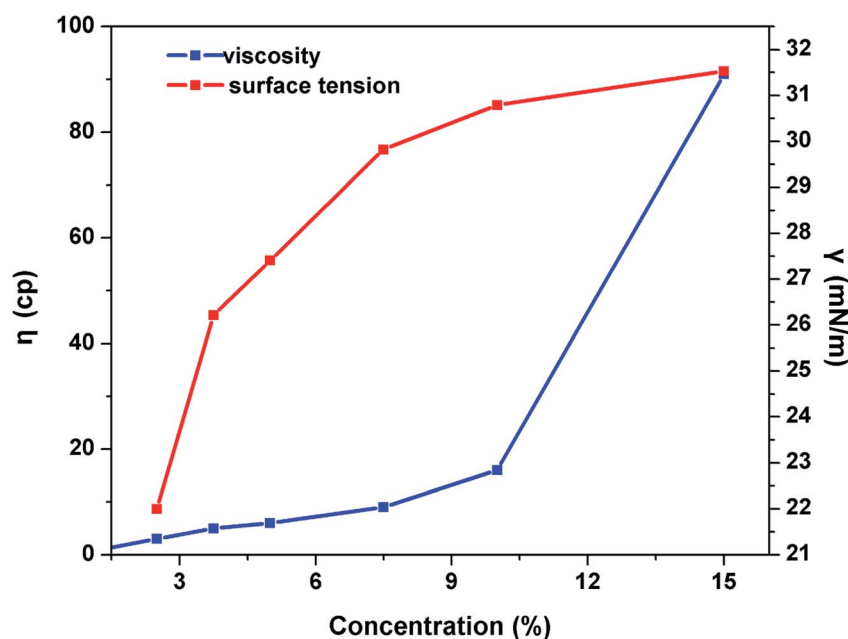
Table 2 The surface tension of the precursor solutions with different solvents

	$CHCl_3$	THF	CH_2Cl_2	HFIP
Surface tension	24.5	22.0	20.7	5.8 (mN m^{-1})
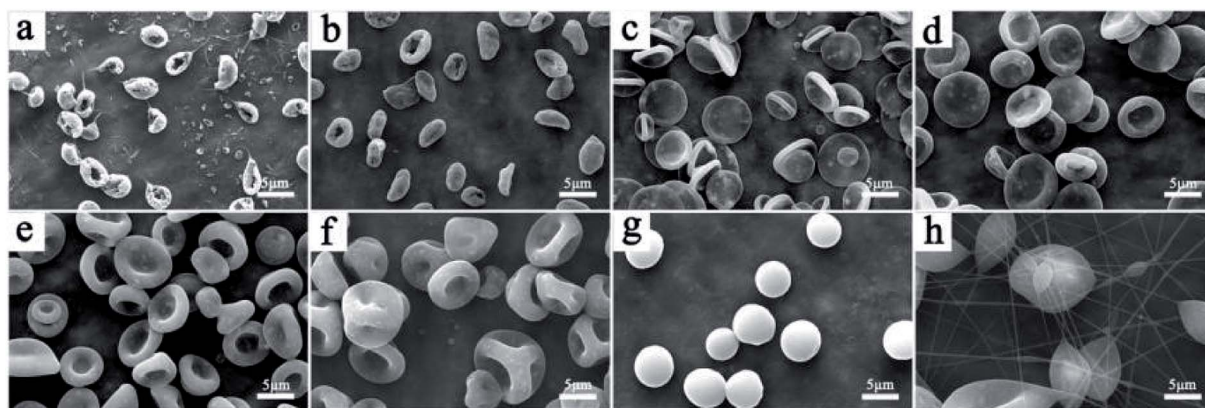
Fig. 4 (A) SEM images of the Fe_3O_4/$TbLa_3(Bim)_{12}$/PLGA composite particles under different PLGA concentrations (a) 0.625%, (b) 1.25%, (c) 2.5%, (d) 3.75%, (e) 5%, (f) 7.5%, (g) 10%, (h) 15%; (B) the relationship of the surface tension and viscosity of the solutions with the change of PLGA concentration.

was lower than the electrostatic repulsion, fibres were easier to produce. A few short fibres appeared along the irregular particles when using CH_2Cl_2 as solution, and more fibres could be observed when HFIP, with low surface tension, was used.

3.1.2 The influence of the PLGA concentration on the RBC-like Fe_3O_4/$TbLa_3(Bim)_{12}$/PLGA composite particles. The effect of the PLGA concentration on the morphology of the RBC-like particles was investigated. Precursor solutions containing 50 mg Fe_3O_4 and 100 mg $TbLa_3(Bim)_{12}$ were electrosprayed with different amounts of PLGA. The SEM images of the particles with different PLGA concentrations were shown in Fig. 4A. At the concentration of 0.625% PLGA, irregular particles were

generated. With the increase of the PLGA concentration, more and more regular particles appeared. The RBC-like particles began to form at 2.5%. When the concentration reached at 7.5%, concave particles with three sides were fabricated. At 10%, a large number of spherical particles were obtained. As concentrations beyond 15%, large spindle-shaped particles accompanying those with the appearance of fibres were produced. The result was consistent with a study on the transition from the roundness of a bead to oval shape.[35] The optimal concentration range to produce RBC-like particles is from 2.5% to 5%.
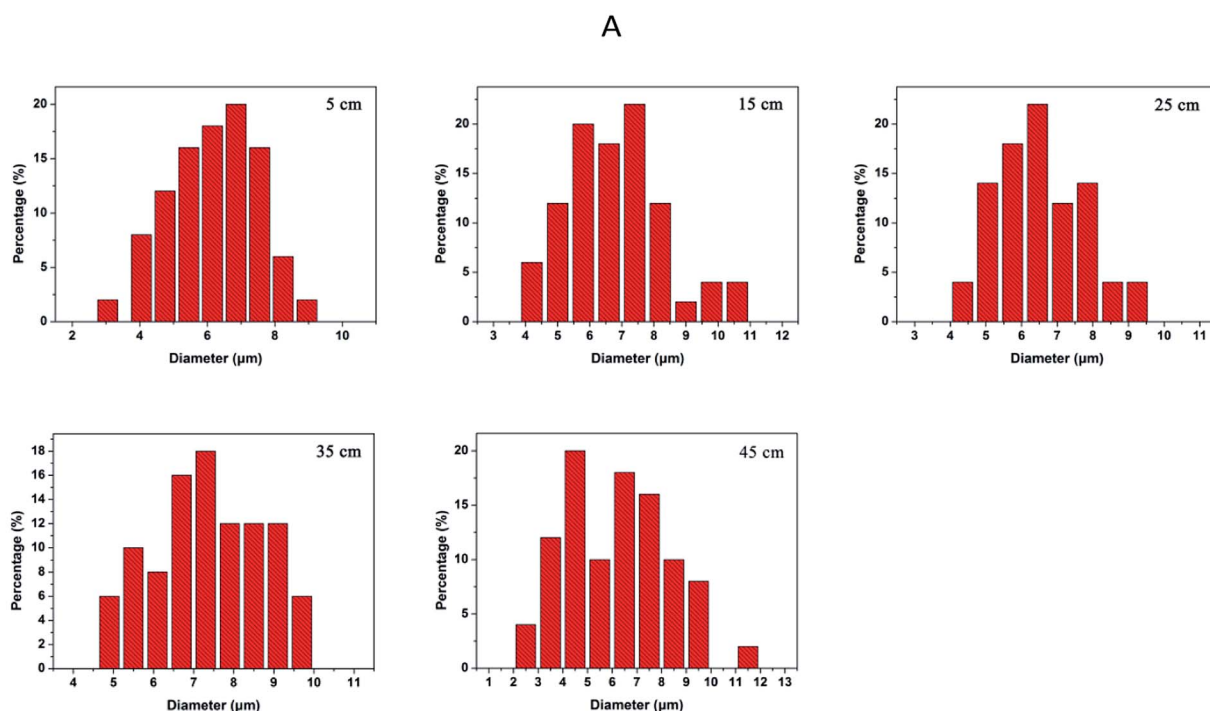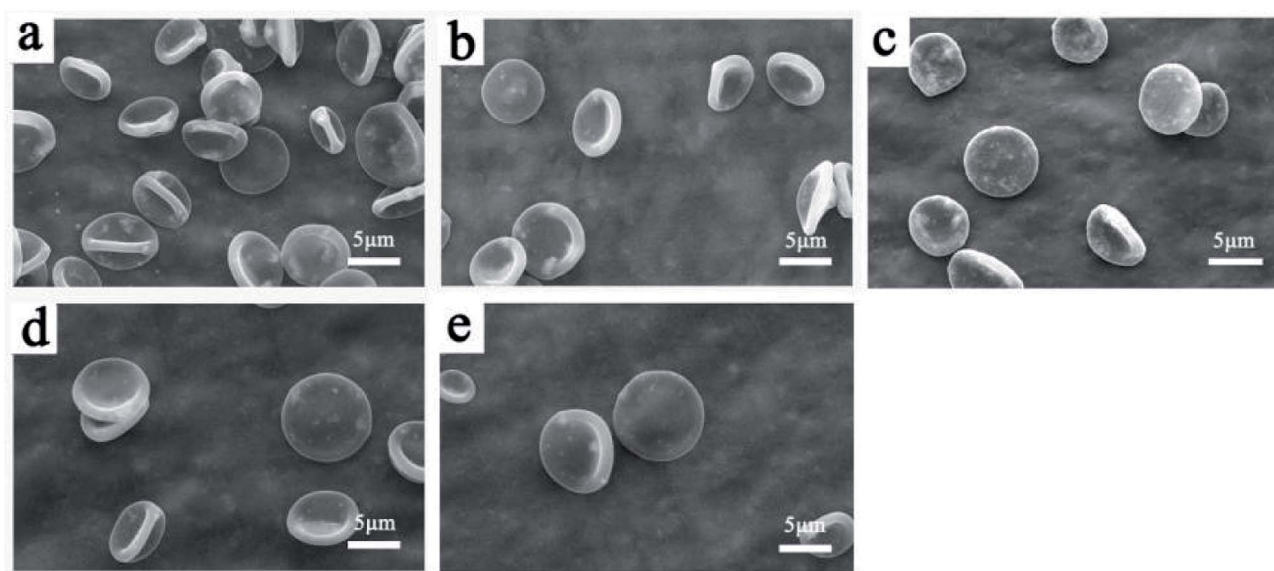
Fig. 5 (A) SEM images of the $Fe_3O_4/TbLa_3(Bim)_{12}$/PLGA composite particles at different distances. (a) 5 cm, (b) 15 cm, (c) 25 cm, (d) 35 cm, (e) 45 cm; (B) the particle size distribution at different collecting distances.

The viscosity and surface tension of the solutions with different PLGA concentrations were shown in Fig. 4B. In areas with low PLGA concentration, the viscosity of solutions was very small, the tangling of molecular chains was insufficient or there was even a lack entanglement, which easily caused the fracture of molecular chains, as a result, the jet flow was likely to form irregular particles rather than fibres. However, as the surface tension gradually increased, occupying the leading position, it contributed to the formation of regular particles. Accordingly, from 2.5% to 5%, RBC particles were obtained. With higher surface tension at 7.5% PLGA concentration, three-side concave particles appeared. When the PLGA concentration reached at 10%, the surface tension continued to increase, while the viscosity increased at low magnitude, and then the spherical
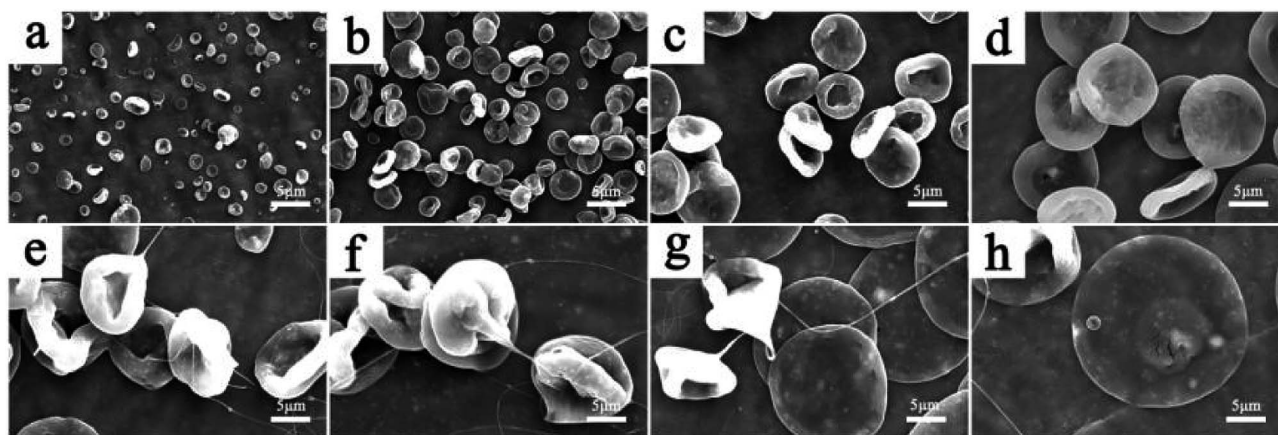
Fig. 6 SEM images of the $Fe_3O_4/TbLa_3(Bim)_{12}/PLGA$ composite particles at different flow rates. (a) 0.1 mL h^{-1}, (b) 0.4 mL h^{-1}, (c) 1.6 mL h^{-1}, (d) 2.4 mL h^{-1}, (e) 3.2 mL h^{-1}, (f) 4.8 mL h^{-1}, (g) 6.0 mL h^{-1}, (h) 7.2 mL h^{-1}.

particles formed easily. At 15% PLGA concentration, the viscosity of the solutions increased dramatically, whereas the rising trend of the surface tension slowed down. At high PLGA concentration, it is observed that spindled-shape particles and even fibres were produced.

3.1.3 The influence of the collecting distance on $Fe_3O_4/TbLa_3(Bim)_{12}/PLGA$ composite particles.

The influence of different collecting distances on the PLGA particle morphology and size was also investigated. The precursor of the 125 mg PLGA, 50 mg Fe_3O_4 and 100 mg $TbLa_3(Bim)_{12}$ in THF were electrosprayed at the collecting distances from 5 to 45 cm. The SEM images and size distribution of the particles were shown in Fig. 5A and B. The images revealed that RBC-like particles could be prepared at the distances from 5 to 45 cm, which suggested that the collecting distance had little effect on the morphology of the RBC-like particles, but rather had its effect on the particles size distribution. The diameter of 50 particles from each sample was measured with the software Nano Measurer 1.2. In the distance from 5 to 35 cm (Fig. 5A(a–c)), the average particles size became larger as the collecting distance increased, with an average diameter of 6.21, 6.75, 6.83 and 7.37 μm, respectively. With the increase of the distance, the electric field force declined, which weakened the stretching of the jet flow and, consequently, resulted in the increase of the diameter. However, at the distance of 45 cm, the average particles size decreased to 6.19 μm. When the distance reached 45 cm, more time was required for the jet flow to stretch sufficiently, and the solvent could completely volatilize, then the smaller particles could be observed, but with a more uneven distribution.

3.1.4 The influence of the solution flow rates on the $Fe_3O_4/TbLa_3(Bim)_{12}/PLGA$ composite particles.

The solution of 2.5% PLGA in THF, 50 mg Fe_3O_4 and 100 mg $TbLa_3(Bim)_{12}$ was electrosprayed at different flow rates and the SEM images of the samples were shown in Fig. 6. The RBC-like particles appeared at the rate of 0.10 mL h^{-1} as shown in Fig. 6, where some irregular particles can also be observed and the particles size is uniformly distributed. The regular RBC-like particles could be obtained at the rate of 0.4, 1.6, and 2.4 mL h^{-1}, and the

diameter of particles increased with increasing flow rate, as shown in Fig. 6b–d. However, the RBC-like PLGA particles became irregular again and were accompanied with a few fibres when the flow rate changed from 3.2 to 6.0 mL h^{-1}, and there even appeared particles with flat shape at 7.2 mL h^{-1}. The high flow rate might lead to the charge accumulation of jet-cone, increasing the jet instability and causing the irregular particles and fibre to appear.[36]

To obtain good RBC-like particles, the following electrospraying factors were chosen in the subsequent study: 2.5% PLGA concentration, THF as solvent, collecting distance of 15 cm and flow rate at 0.8 mL h^{-1}. The size distribution of RBC-like particles was shown in Fig. 7. The average hydrodynamic diameter was 6.5 μm.

3.2 Stability evaluation under ambient condition

The stability of RBC-like $Fe_3O_4/TbLa_3(Bim)_{12}/PLGA$ particles in PBS (1 mg mL^{-1}) was examined by UV-VIS-NIR

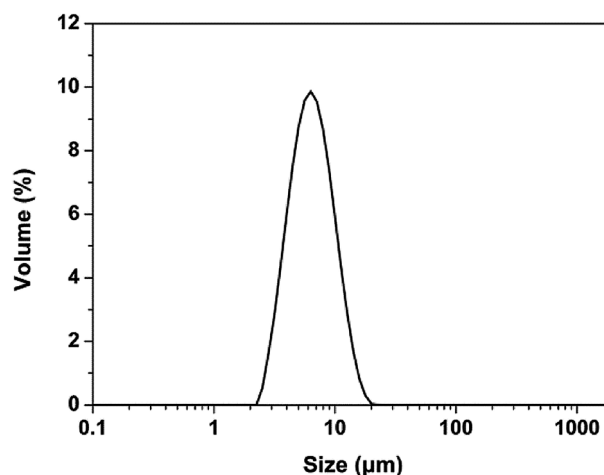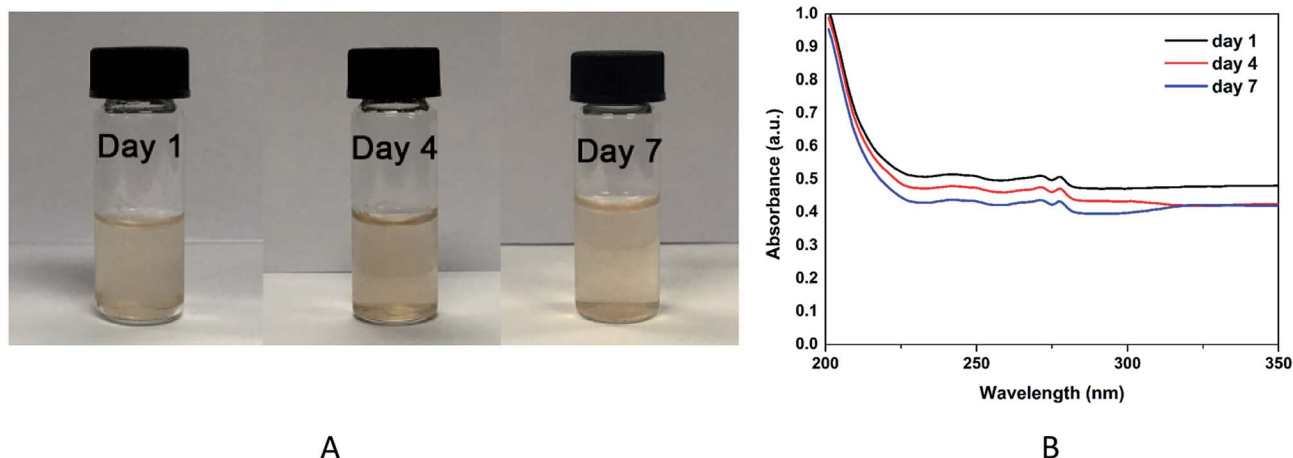**Fig. 7** Size distribution of RBC-like $Fe_3O_4/TbLa_3(Bim)_{12}/PLGA$ composite particles.

Fig. 8 Stability evaluation under ambient condition. (A) Photographs and (B) absorption spectra of RBC-like $Fe_3O_4/TbLa_3(Bim)_{12}$/PLGA particles with the same concentration after storing in PBS for different periods of time.

spectrophotometer at predetermined time intervals(1, 4 and 7 days). As shown in Fig. 8A, the colour of sample solution was similar and there was no significant change appeared. The UV absorbance spectra (Fig. 8B) showed there were several weak absorption peaks between 240 and 280 nm. Along with the time, the absorbance intensities of RBC-like $Fe_3O_4/TbLa_3(Bim)_{12}$/ PLGA particles slightly decreased, which demonstrated that the RBC-like particles were biodegradable.

3.3 Infrared analysis

The FTIR spectra of Bim, $TbLa_3(Bim)_{12}$, PLGA and $Fe_3O_4/TbLa_3(Bim)_{12}$/PLGA were displayed in Fig. 9. The peaks of Bim at 3061, 1454.55, 1409.93, 1243.89 and 748.25 cm^{-1} represent the C–H stretching vibration of the benzene ring, the C=N stretching vibration, the in-plane deformation of the benzimidazole ring, the in-plane C–H deformation and the out-of-plane C–H bending vibration, respectively. The infrared spectrum of $TbLa_3(Bim)_{12}$ was distinctly different

from the spectrum of the Bim ligand. The peak at 3061 cm^{-1} disappeared, while the peaks at 1409.93 cm^{-1} and 1243.89 cm^{-1} red-shifted to 1504.11 cm^{-1} and 1398.09 cm^{-1} and the peak at 748.25 cm^{-1} blue-shifted to 720.36 cm^{-1}. The shifts of the above peaks indicated that the Bim ligand was successfully bound to Tb^{3+} and La^{3+}. Additionally, a wide O–H stretching vibration absorption peak located at 3555 cm^{-1} occurred, which indicated that there was crystal water generated in the $TbLa_3(Bim)_{12}$. Compared with $TbLa_3(Bim)_{12}$, a strong peak in the spectrum of $Fe_3O_4/TbLa_3(Bim)_{12}$/PLGA at 1761.58 cm^{-1} was due to the C=O stretching vibration present in PLGA, and the absorption peaks at 1184.55 cm^{-1} and 1096.71 cm^{-1} were assigned to the C–O stretching vibration of PLGA. Some peaks that appeared in $TbLa_3(Bim)_{12}$ were not observed in the $Fe_3O_4/TbLa_3(Bim)_{12}$/PLGA, which is probably covered by the strong signals of PLGA. Overall, $TbLa_3(Bim)_{12}$ was successfully encapsulated by the RBC-like PLGA particles.
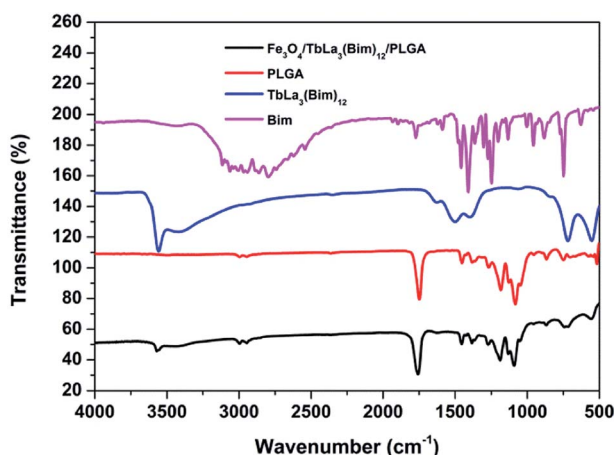

Fig. 9 FTIR spectra of Bim, $TbLa_3(Bim)_{12}$, PLGA and RBC-like $Fe_3O_4/TbLa_3(Bim)_{12}$/PLGA composite particles.
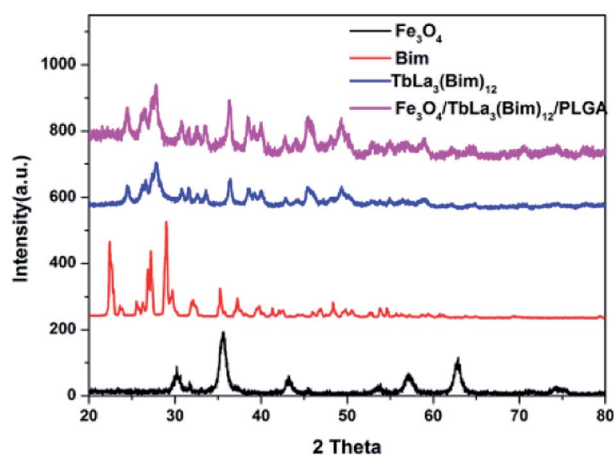
Fig. 10 XRD patterns of Fe_3O_4 MNPs, Bim, $TbLa_3(Bim)_{12}$ and the RBC-like $Fe_3O_4/TbLa_3(Bim)_{12}$/PLGA composite particles.
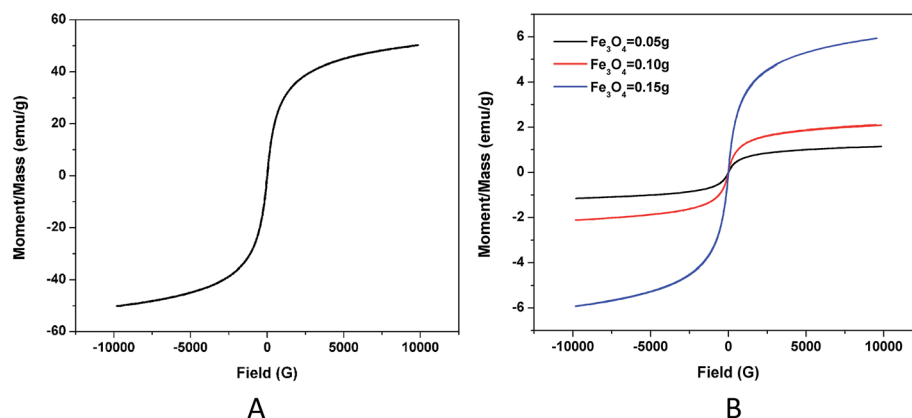
Fig. 11 (A) Hysteresis loop of pure Fe_3O_4; (B) hysteresis loops of the RBC-like $Fe_3O_4/TbLa_3(Bim)_{12}/PLGA$ composite particles with different amounts of Fe_3O_4.

3.4 XRD analysis

The XRD patterns of Fe_3O_4, Bim, $TbLa_3(Bim)_{12}$ and the RBC-like $Fe_3O_4/TbLa_3(Bim)_{12}/PLGA$ composite particles were shown in Fig. 10. For the Fe_3O_4 MNPs, all the intense peaks could be well indexed to the cubic phase of Fe_3O_4 (JCPDS no. 74-0748), and no other characteristic peaks were observed, indicating no impurities like FeO(OH) and Fe_2O_3 were produced. The spectrum of $TbLa_3(Bim)_{12}$ had weaker crystalline peaks than those of Bim, suggesting that the reaction of Tb^{3+}, La^{3+} and Bim had already been completed. For $Fe_3O_4/TbLa_3(Bim)_{12}/PLGA$, the diffraction pattern included peaks of both Fe_3O_4 MNPs and $TbLa_3(Bim)_{12}$, indicating that they have been successfully encapsulated by PLGA.

3.5 The magnetic properties of the RBC-like $Fe_3O_4/$ $TbLa_3(Bim)_{12}/PLGA$ composite particles

To study the magnetic properties of the $Fe_3O_4/TbLa_3(Bim)_{12}/$ PLGA particles and the influence of different amounts of Fe_3O_4 MNPs in the particles, the hysteresis loops of the Fe_3O_4 MNPs and RBC-like $Fe_3O_4/TbLa_3(Bim)_{12}/PLGA$ particles under an applied field of 10 kOe were shown in Fig. 11. The saturation magnetization of the pure Fe_3O_4 MNPs was 51 emu g^{-1}. The magnetic properties of the RBC-like $Fe_3O_4/TbLa_3(Bim)_{12}/PLGA$ composite particles depended on the contents of the magnetic substance in the particles. When the contents of the Fe_3O_4

MNPs varied from 50 mg to 150 mg, the value of saturation magnetization increased from 1.14 to 5.94 emu g^{-1}. These results indicated that the composite particles had adequate magnetic response for biomedical applications, and magnetic response could be tuned by adding various amounts of Fe_3O_4 MNPs.

The magnetic response capability of particles (S6 in Table 1) was tested by adding particles to A549 cell culture medium while using a magnet. The results visualized with a fluorescent microscope were shown in Fig. 12. Before adding the magnet, it was observed that particles were uniformly distributed in a Petri dish. After placing a magnet in the side of the Petri dish, more particles appeared at the side near the magnet and, on the contrary, a few particles sparsely distributed at the other side. The magnetism of the particles still existed even when incubated with cells for 1 or more days, suggesting the possibility that the RBC-like $Fe_3O_4/TbLa_3(Bim)_{12}/PLGA$ composite particles can be additionally applied in magnetic targeting *in vivo*.

3.6 The fluorescent properties of the RBC-like $Fe_3O_4/$ $TbLa_3(Bim)_{12}/PLGA$ composite particles

The fluorescent properties of the RBC-like $Fe_3O_4/TbLa_3(Bim)_{12}/$ PLGA composite particles were studied at the excitation wavelength of 350 nm. The emission spectra of RBC-like particles encapsulating different amounts of $TbLa_3(Bim)_{12}$ were displayed in Fig. 13A. The fluorescent intensity was enhanced by

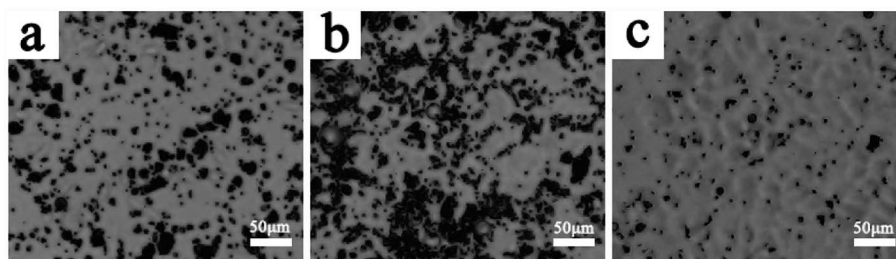**Fig. 12** Fluorescent microscope images of A549 cells incubated with the RBC-like $Fe_3O_4/TbLa_3(Bim)_{12}/PLGA$ composite particles under the effect of a magnet. (a) Without magnet, (b) near magnet, (c) far from magnet.
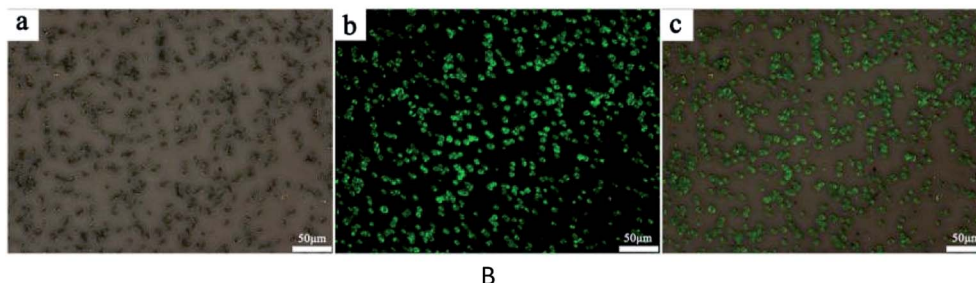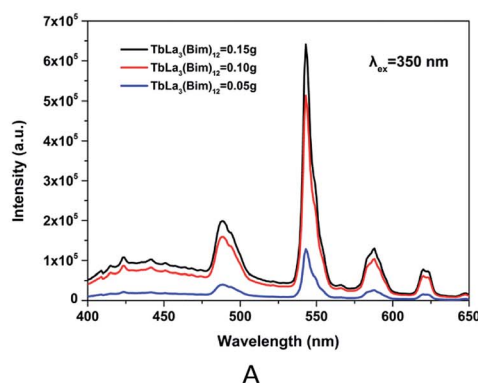
Fig. 13 (A) Emission spectra of the RBC-like Fe_3O_4/$TbLa_3(Bim)_{12}$/PLGA composite particles with different amounts of $TbLa_3(Bim)_{12}$; (B) fluorescent microscope images of the RBC-like Fe_3O_4/$TbLa_3(Bim)_{12}$/PLGA composite particles. (a) Bright-field image, (b) fluorescent image (c) the overlay image.

the increase of the content of $TbLa_3(Bim)_{12}$. When the content of $TbLa_3(Bim)_{12}$ was 50 mg, the particles exhibited the lowest fluorescent intensity. Then, the fluorescent intensity increased markedly when the content of $TbLa_3(Bim)_{12}$ reached to 100 mg, which was two times more than the former one. When 150 mg $TbLa_3(Bim)_{12}$ was used, the fluorescent intensity was the strongest. The emission peaks at 489, 543, 588 and 620 nm can be assigned to $^5D_4 \rightarrow {}^7F_6$, $^5D_4 \rightarrow {}^7F_5$, $^5D_4 \rightarrow {}^7F_4$ and $^5D_4 \rightarrow {}^7F_3$ of Tb^{3+}, and the peak at 543 nm exhibited the predominant emission intensity, which was just in the range of the green light wavelength band. The bright-field image, fluorescent image and the overlay image of the RBC-like particles were separately shown in Fig. 13B. The intense green fluorescence revealed that the RBC-like Fe_3O_4/$TbLa_3(Bim)_{12}$/PLGA composite particles had excellent fluorescent properties, which was in accord with the predominant emission peak.

After the particles were added to the A549 cell culture medium for 24 h, the cell imaging was achieved by fluorescent

microscope. A bright green light was visualized in the fluorescent image (Fig. 14b), corresponded to the maximum emission wavelength of 543 nm, indicating that the Fe_3O_4/$TbLa_3(Bim)_{12}$/PLGA composite particles exhibited an excellent fluorescent property and could potentially function for drug labeling even after being incubated with cells for 24 h or more hours. Moreover, no fluorescence quenching appeared after 24 h. Remarkably, the particles mainly centralized on the cells (Fig. 14a and c), revealing the outstanding targeting ability towards cells. This might be because the RBC morphology was easily attached to the soft cells.

3.7 The hydrophobicity-hydrophilicity of the RBC-like Fe_3O_4/$TbLa_3(Bim)_{12}$/PLGA composite particles

For most biological system, dispersion of particles in the aqueous phase is required. Many researchers found that cell adherence growth greatly depends on the increase in
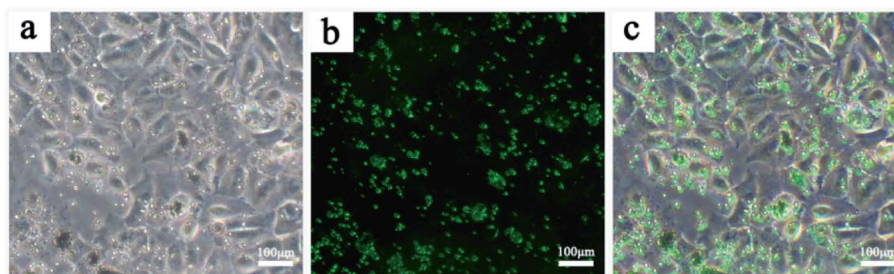

Fig. 14 Fluorescent microscope images of A549 cells incubated with the RBC-like Fe_3O_4/$TbLa_3(Bim)_{12}$/PLGA composite particles. (a) Bright-field image, (b) fluorescent image (c) the overlay of the bright-field and fluorescent image.
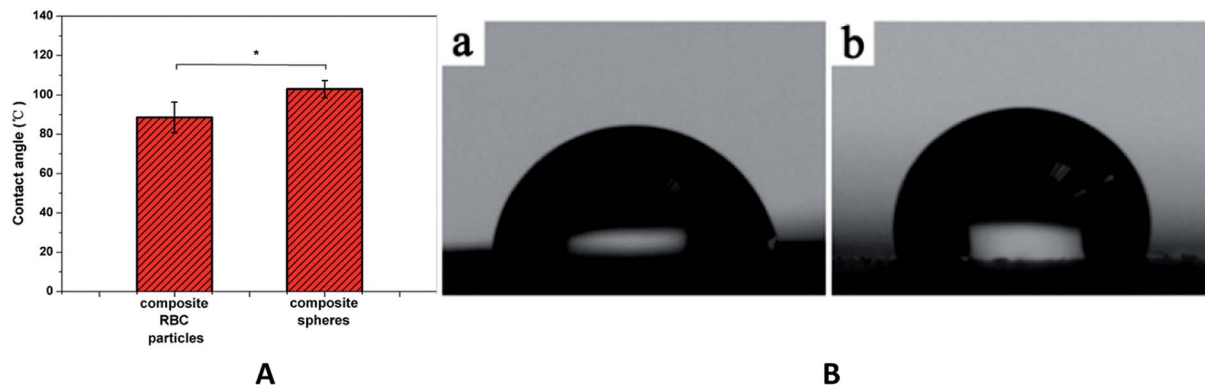
Fig. 15 (A) Contact angles of two different samples. "*" Indicates significant difference of $p < 0.05$; (B) images of water droplets on different samples. (a) RBC-like $Fe_3O_4/TbLa_3(Bim)_{12}/PLGA$ composite particles, (b) $Fe_3O_4/TbLa_3(Bim)_{12}/PLGA$ composite spheres.

hydrophobicity–hydrophilicity.[37] It was reported that moderate contact angle (40–70°) would be better to adsorb cell adhesive protein, which caused cell attachment.[38] PLGA has been widely used in biomedical application. However, the hydrophobicity limited the further usage. Therefore, it was necessary to explore the hydrophobicity–hydrophilicity of biomaterials synthesized by PLGA. To examine the hydrophobicity–hydrophilicity of the RBC-like PLGA particles, we measured the contact angles of the RBC-like $Fe_3O_4/TbLa_3(Bim)_{12}/PLGA$ composite particles (S6 in Table 1) and the $Fe_3O_4 \ TbLa_3(Bim)_{12}/PLGA$ composite spheres. The composite spheres were electrosprayed with 10% PLGA, and other dosages were consistent with sample (S6). As shown in Fig. 15, the contact angles of the RBC-like $Fe_3O_4/TbLa_3(Bim)_{12}/PLGA$ composite particles and the $Fe_3O_4/TbLa_3(Bim)_{12}/PLGA$ composite spheres were 88.53° and 103.92° respectively. The RBC-like particles exhibited a smaller contact angle than the spheres, which increased the hydrophobicity of the particles. The results suggested that the RBC-like $Fe_3O_4/TbLa_3(Bim)_{12}/PLGA$ composite particles may exhibit better biocompatibility between materials and cells.

3.8   The cytotoxicity of the RBC-like $Fe_3O_4/TbLa_3(Bim)_{12}/PLGA$ composite particles

The cytotoxicity of the RBC-like $Fe_3O_4/TbLa_3(Bim)_{12}/PLGA$ composite particles was determined by the CCK-8 assay. The viability of untreated A549 cells was assumed to be 100%. The results revealed that the cell viability of all experimental groups at different concentrations from 7.81 to 1000 μg mL^{-1} was declined to some extent after incubation for 24 h, as shown in Fig. 16. Nevertheless, cell viability was still more than 90% even at the high concentration of 1000 μg mL^{-1} of the RBC-like $Fe_3O_4/TbLa_3(Bim)_{12}/PLGA$ composite particles. The CCK-8 assay results demonstrated that the $Fe_3O_4/TbLa_3(Bim)_{12}/PLGA$ composite particles had low cytotoxicity. Furthermore, with the increase of the concentration, the cell viability showed no significant change. The $Fe_3O_4/TbLa_3(Bim)_{12}/PLGA$ composite particles would have excellent biocompatibility in additional biomedical applications.

3.9   Hemolytic activity of RBC-like $Fe_3O_4/TbLa_3(Bim)_{12}/PLGA$ composite particles

A hemolysis assay was used to determine the toxicity of RBC-like $Fe_3O_4/TbLa_3(Bim)_{12}/PLGA$ composite particles on RBCs. Hemolysis results for samples (at a range of 7.81 to 250 μg mL^{-1}) were given in Fig. 17. All samples hemolytic rates were below 5%, which was thought to be the risky ratio described in ISO/TR7405 standard.[39] Photographs of precipitated RBCs were also given, there was no obvious hemoglobin released from damaged cells, demonstrating that there was excellent blood biocompatibility between materials and RBCs.

3.10   Protein corona assay

Due to large surface-to-volume ratio and surface properties, micro and nanoparticles will rapidly absorb biomolecules to form 'protein corona'. This protein corona, which provides particles with a 'biological identity', not only alters the properties of particles but also determines subsequent physiological responses.[40] Thus, it is necessary to study the non-specific
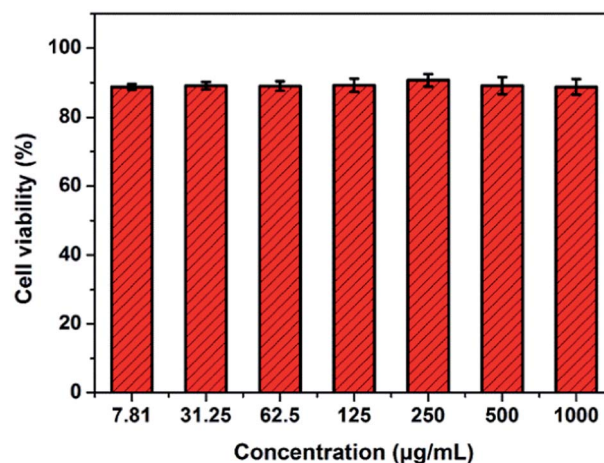

Fig. 16 *In vitro* A549 cells relative viabilities normalized to the untreated control after incubation for 24 h with different concentrations of the RBC-like $Fe_3O_4/TbLa_3(Bim)_{12}/PLGA$ composite particles.
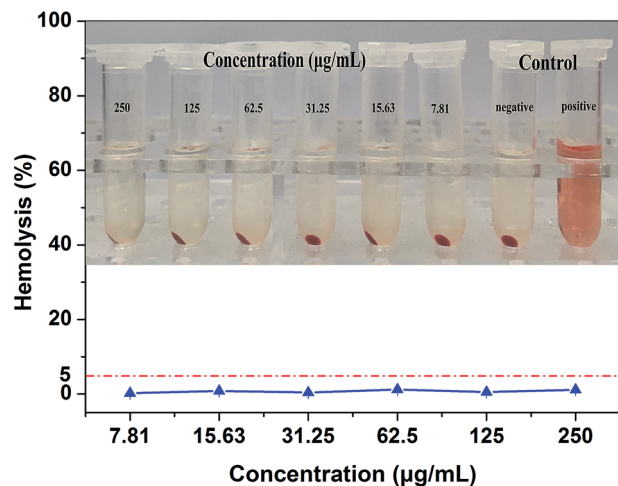
Fig. 17 Hemolysis rate and photographs of RBC-like Fe$_3$O$_4$/TbLa$_3$(Bim)$_{12}$/PLGA composite particles at different concentration between 7.81 and 250 µg mL^{-1}.
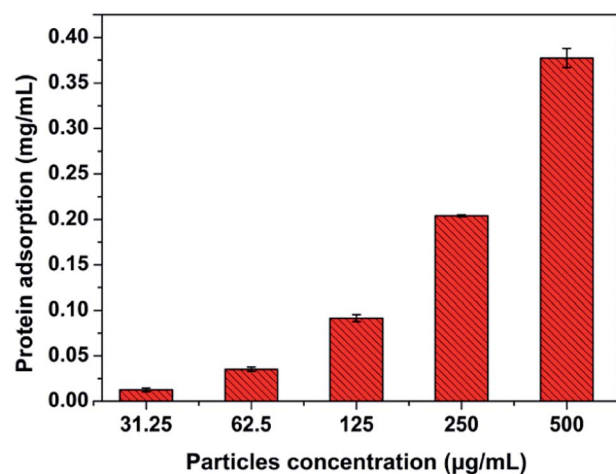
Fig. 18 Protein adsorption of RBC-like Fe$_3$O$_4$/TbLa$_3$(Bim)$_{12}$/PLGA composite particles.

protein adsorption on particles. The protein corona was determined in RPMI-1640 culture medium with 10% FBS by BCA Protein Assay Kit. The results of protein adsorption were shown in Fig. 18. The protein adsorption increased with the concentration of particles, which suggested that a proper particles concentration should be considered to utilize or minimize the influence of protein corona.

4. Conclusions

The RBC-like magnetic-fluorescent bifunctional Fe$_3$O$_4$/TbLa$_3$(Bim)$_{12}$/PLGA composite particles were successfully prepared by electrospraying. The generation of RBC-like structure was mainly related to the properties of the solutions, such as the choice of solvent, PLGA concentrations, and flow rate of the solutions. However, external control variable like collecting distance had smaller influence on the formation of the RBC-like structure, mainly affecting the particles

size. In this study, the optimal parameters to obtain the RBC-like particles were using THF as solvent, 2.5–5% PLGA concentration, 15 cm collecting distance and 0.8 mL h^{-1} flow rate. Several results suggested that the RBC-like Fe$_3$O$_4$/TbLa$_3$(Bim)$_{12}$/PLGA composite particles have excellent, tunable magnetism and fluorescent properties. The RBC morphology could increase the hydrophilicity of the particles. Finally, the cells experiments showed that the RBC-like particles have low toxicity and excellent biocompatibility. The fluorescence of materials can be clearly observed while incubated with A549 cells, whereby the accurate drug tracking can be achieved. Additionally, under the influence of a magnetic field, the RBC-like particles showed excellent magnetic response. This RBC-like magnetic-fluorescent bifunctional Fe$_3$O$_4$/TbLa$_3$(Bim)$_{12}$/PLGA composite particles offer promising potential for application in the biomedical field, especially in DDS.

Conflicts of interest

There are no conflicts to declare.

Acknowledgements

References

1 H. Yadav, P. Kumar, V. Sharma, G. Sharma, B. Raza and O. P. Katare, *RSC Adv.*, 2016, **6**, 53351–53357.
2 G. Minigo, A. Scholzen, C. K. Tang, J. C. Hanley, M. Kalkanidis, G. A. Pietersz, V. Apostolopoulos and M. Plebanski, *Vaccine*, 2007, **25**, 1316–1327.
3 L. J. Lu, Y. Wang, M. H. Cao, M. W. Chen, B. L. Lin, X. H. Duan, F. Zhang, J. J. Mao, X. T. Shuai and J. Shen, *RSC Adv.*, 2017, **7**, 15041–15052.
4 D. Y. Tang, X. Zhao, T. Yang and C. Wang, *RSC Adv.*, 2018, **8**, 380–389.
5 Y. F. Ma, Y. Ji, M. L. You, S. R. Wang, Y. Q. Dong, G. R. Jin, M. Lin, Q. Wang, A. Li, X. H. Zhang and F. Xu, *Acta Biomater.*, 2016, **42**, 199–208.
6 S. F. Wang, C. T. Zhao, P. Liu, Z. Wang and J. S. Ding, *RSC Adv.*, 2018, **8**, 444–453.
7 Y. Hao, Y. X. Huang, Y. Q. He, J. R. Peng, L. J. Chen, X. Hu and Z. Y. Qian, *RSC Adv.*, 2016, **6**, 13698–13709.
8 D. M. Richards and R. G. Endres, *Proc. Natl. Acad. Sci. U. S. A.*, 2016, **113**, 6113–6118.
9 K. Vahidkhah and P. Bagchi, *Soft Matter*, 2015, **11**, 2097–2109.

10 J. Carolyn, V. S. Vladimir, B. Mark, R. M. Vladimir and D. D. Thomas, *Curr. Pharm. Des.*, 2016, **22**, 1259–1273.

11 Y. Geng, P. Dalhaimer, S. S. Cai, R. Tsai, M. Tewari, T. Minko and D. E. Discher, *Nat. Nanotechnol.*, 2007, **2**, 249–255.

12 B. Godin, C. Chiappini, S. Srinivasan, J. F. Alexander, K. Yokoi, M. Ferrari, P. Decuzzi and X. W. Liu, *Adv. Funct. Mater.*, 2012, **22**, 4225–4235.

13 P. Decuzzi and M. Ferrari, *Biophys. J.*, 2008, **94**, 3790–3797.

14 P. Decuzzi and M. Ferrari, *Biomaterials*, 2006, **27**, 5307–5314.

15 J. P. Best, Y. Yan and F. Caruso, *Adv. Healthcare Mater.*, 2012, **1**, 35–47.

16 A. F. Galvao, T. Petta, N. Flamand, V. R. Bollela, C. L. Silva, L. R. Jarduli, K. C. R. Malmegrim, B. P. Simoes, L. A. B. Moraes and L. H. Faccioli, *Anal. Bioanal. Chem.*, 2016, **408**, 3613–3623.

17 S. Mitragotri and J. Lahann, *Nat. Mater.*, 2009, **8**, 15–23.

18 V. Kozlovskaya, J. F. Alexander, Y. Wang, T. Kuncewicz, X. W. Liu, B. Godin and E. Kharlampieva, *ACS Nano*, 2014, **8**, 5725–5737.

19 T. J. Merkel, S. W. Jones, K. P. Herlihy, F. R. Kersey, A. R. Shields, M. Napier, J. C. Luft, H. L. Wu, W. C. Zamboni, A. Z. Wang, J. E. Bear and J. M. Desimone, *Proc. Natl. Acad. Sci. U. S. A.*, 2011, **108**, 586–591.

20 J. B. Fan, Y. Y. Song, H. F. Li, J. P. Jia, X. L. Guo and L. Jiang, *J. Mater. Chem. B*, 2014, **2**, 3911–3914.

21 Y. H. Lee, F. Mei, M. Y. Bai, S. L. Zhao and D. R. Chen, *J. Controlled Release*, 2010, **145**, 58–65.

22 W. P. Lv, K. J. Lee, S. Hwang, T. H. Park, F. B. Zhang and J. Lahan, *Part. Part. Syst. Charact.*, 2013, **30**, 936–939.

23 S. Sahoo, W. C. Lee, J. C. Goh and S. L. Toh, *Biotechnol. Bioeng.*, 2010, **106**, 690–698.

24 J. W. Xie, J. Jiang, P. Davoodi, M. P. Srinivasan and C. H. Wang, *Chem. Eng. Sci.*, 2015, **125**, 32–57.

25 K. Hayashi, K. Ono, H. Suzuki, M. Sawada, M. Moriya, W. Sakamoto and T. Yogo, *Small*, 2010, **6**, 2384–2391.

26 C. H. Park, N. Chung and J. Lee, *J. Colloid Interface Sci.*, 2011, **361**, 423–428.

27 X. J. Ju, X. X. Wang, Z. Liu, R. Xie, W. Wang and L. Y. Chu, *Particuology*, 2017, **30**, 151–157.

28 X. D. Lu, *et al.*, *Mater. Sci. Eng., C*, 2018, **82**, 190–196.

29 D. E. Hodges, K. M. McNally and A. J. Welch, *J. Biomed. Opt.*, 2001, **6**, 427–431.

30 L. Han, Q. l. Ma and X. T. Dong, *RSC Adv.*, 2015, **5**, 95674–95681.

31 S. Fischer, C. Foerg, S. Ellenberger, H. P. Merkle and B. Gander, *J. Controlled Release*, 2006, **111**, 135–144.

32 W. Wang, D. Xu, X. J. Wei and K. Z. Chen, *Int. J. Nanomed.*, 2014, **9**, 4879–4891.

33 P. Li, K. Li, X. F. Niu and Y. B. Fan, *RSC Adv.*, 2016, **6**, 99034–99043.

34 A. Yildirim, E. Ozgur and M. Bayindir, *J. Mater. Chem. B*, 2013, **1**, 1909–1920.

35 J. Y. Lin, B. Ding, J. Y. Yu and Y. Hsieh, *ACS Appl. Mater. Interfaces*, 2010, **2**, 521–528.

36 C. Wang, C. H. Hsu and J. H. Lin, *Macromolecules*, 2006, **39**, 7662–7672.

37 J. H. Lee, G. Khang, J. W. Lee and H. B. Lee, *J. Colloid Interface Sci.*, 1998, **205**, 323–330.

38 Y. Wan, W. Chen, J. Yang, J. Bei and S. Wang, *Biomaterials*, 2003, **24**, 2195–2203.

39 Y. Wang, N. Han, Q. Zhao, L. Bai, J. Li, T. Jiang and S. Wang, *Eur. J. Pharm. Sci.*, 2015, **72**, 12–20.

40 Q. Dai, N. Z. Bertleff, J. A. Braunger, M. Björnmalm, C. J. Cortez and F. Caruso, *Adv. Healthcare Mater.*, 2018, **7**, 1700575.